

Article

Restoration of Grassland Improves Soil Infiltration Capacity in Water-Wind Erosion Crisscross Region of China's Loess Plateau

Xiuzi Ren ¹, Xiaohong Chai ¹, Yuanyuan Qu ¹, Yuanhui Xu ¹, Farhat Ullah Khan ², Junfeng Wang ¹, Palixiati Geming ¹, Weiwei Wang ¹, Qi Zhang ¹, Qinxuan Wu ¹, Xuexuan Xu ^{2,*} and Feng Du ^{2,*}

¹ College of Grassland Agriculture, Northwest A&F University, Xianyang 712100, China; 2021051671@nwafu.edu.cn (X.R.); cxh902@nwafu.edu.cn (X.C.); quyuanqu@nwafu.edu.cn (Y.Q.); xuyuanhui@nwafu.edu.cn (Y.X.); 2021060664@nwafu.edu.cn (J.W.); palixiati@nwafu.edu.cn (P.G.); wangweiwei422@nwafu.edu.cn (W.W.); 1228@nwafu.edu.cn (Q.Z.); 2022051699@nwafu.edu.cn (Q.W.)

² Institute of Soil and Water Conservation, Northwest A&F University, Xianyang 712100, China; farhatk304@gmail.com

* Correspondence: xuxuexuan@nwsuaf.edu.cn (X.X.); dufeng@nwafu.edu.cn (F.D.)

Abstract: Soil water infiltration is a key mechanism for meeting plant water demand and groundwater recharge cycles; however, unreasonable land use practices cause reduced infiltration capacity and greater soil erosion. To date, differences in the properties of aeolian sandy soil and Pisha sandstone soil under different utilization methods as well as in soil properties, aggregates, and infiltration among kind of soil types, remain poorly understood. In this work, 54 soil samples of cropland and grassland were selected to identify the unique characteristics of soil infiltration processes under transition from cropland to grassland and contributions of soil properties to soil infiltrability in the Loess Plateau of China. The results showed that converting cropland to grassland could enhance the stable infiltration capacity of shallow soils of aeolian sandy soil and loess soil by 43.6% and 35.7%, respectively. Compared with cropland, the root properties and soil aggregate formation of the three soil types increased during grassland use, with the largest increase in soil organic matter content (32.14%) and total porosities (6.4%). As determined by the ring knife method, the saturated infiltration capacity of Pisha sandstone soil was significantly lower than in aeolian sandy soil and loess soil ($p < 0.5$). Moreover, its saturated infiltration capacity of cropland was better than grassland. Spearman's correlation analysis and structural equation modeling (SEM) revealed that soil infiltration capacity appeared to be the most influenced by soil organic matter, and aggregate structure. These results highlight that fifteen years of returning cropland to grassland is not enough to affect the infiltration ability of deep soil (≥ 20 cm), and this improvement requires longer term maintenance.

Keywords: land use change; soil infiltration rate; saturated hydraulic conductivity; structural equation modeling



Citation: Ren, X.; Chai, X.; Qu, Y.; Xu, Y.; Khan, F.U.; Wang, J.; Geming, P.; Wang, W.; Zhang, Q.; Wu, Q.; et al. Restoration of Grassland Improves Soil Infiltration Capacity in Water-Wind Erosion Crisscross Region of China's Loess Plateau. *Land* **2023**, *12*, 1485. <https://doi.org/10.3390/land12081485>

Academic Editors: Carlos Rogério Mello, Vincent Chaplot, Daniel Bucur and Lilian Niacșu

Received: 17 May 2023

Revised: 19 July 2023

Accepted: 22 July 2023

Published: 27 July 2023



Copyright: © 2023 by the authors. Licensee MDPI, Basel, Switzerland. This article is an open access article distributed under the terms and conditions of the Creative Commons Attribution (CC BY) license (<https://creativecommons.org/licenses/by/4.0/>).

1. Introduction

The Loess Plateau has been subjected to severe soil erosion and water loss, since the implementation of “returning cropland to forest” [1,2], the land use of the Loess Plateau has changed dramatically. However, the soil degradation of structural properties and decrease in infiltration capacity were caused by a change in unreasonable land use [3–5]. Previous studies have focused on the problems of restricted vegetation growth, dry soil layer formation, and increased soil erosion in the process of returning farmland to forest [6]. In the construction of forest and grass vegetation on the Loess Plateau, there has always been a problem of prioritizing trees over shrubs [7]. Creating a large area of tree forests results in soil moisture deficiency and insufficient and unbalanced fertility, which in turn affects tree growth, leading to a large area of artificial forests becoming “little old trees” [8–10]. Currently, strengthening the return of farmland to grassland, implementing artificial grass planting and closing the mountains to cultivate grassland have been regarded as ecological

environment construction measures with less investment and quicker benefits [11]. Nevertheless, there is still a lack of research on the response of soil infiltration during the process of converting farmland to grassland [12]. Therefore, studies on how changes in land use impact soil infiltrability may be beneficial for the sustainable management of the ecological environment in the Loess Plateau region [13].

Many studies have shown that the soil water infiltration process is influenced both by plant root systems (mainly measured as root length density, root biomass, root surface area, and root volume) and soil properties (including soil texture, soil aggregate stability, soil porosity, bulk density, and soil organic matter) [14–17]. Pore structure between soil particles and aggregates also facilitates infiltration of soil moisture [18]. After studying the infiltration rate under different land use modes in the loess hilly area, it was found that the soil hydraulic properties of grasslands are better than those of agri-cultural land and forest land, specifically manifested as a decrease in soil bulk density, an increase in large aggregate (>0.25 mm) content, and aggregate stability [19,20]. Previous studies have begun to investigate the complex relationships between root characteristics and soil properties and their effects on infiltration in China's Yangtze River Basin and Tibetan Plateau [21–23]. However, studies on how soil aggregate's structure and porosity affect infiltration in different parent soils under different land use types remain poorly understood, and the contribution of changes in soil structure to hydraulic properties are often difficult to quantify [24]. Improvement of soil structure and increase in organic matter jointly promote soil infiltration. The pore structure between soil particles and large aggregates can promote water infiltration. The research on the mechanism affecting soil infiltration is helpful to understand the relationship between soil infiltration capacity and vegetation restoration process, and then provide a scientific basis for the regulation of the policy of Grain for Green and grassland.

Soil texture influences the creation of specific-size aggregates, further stimulating larger aggregate sizes and inter-aggregate pores, which are crucial for the formation of inter-particle pore space [25,26]. Three soil types are mainly distributed in the water-wind erosion crisscross region of China's Loess Plateau: aeolian sandy soil, loess soil and Pisha sandstone. Aeolian sandy soil has a loose texture, poor structure, water retention, and fertilizer retention [27]. Pisha sandstone is as hard as a stone when dry, but becomes soft as mud when wet [28]. Although the initial infiltration capacity of all three soil types is excellent [29], there are few studies on the differences in infiltration capacity of the three soil types after abandoned cropland [30]. At present, domestic research results on soil infiltration laws are relatively abundant, and the research areas are mostly concentrated in loess areas, purple soil areas, and sandy lands [31,32]. However, there are relatively few studies on the Pisha sandstone area. Especially, the influence mechanism of soil factors on the infiltration process is not yet clear [33]. Based on the above background, this study selects different parent soils under different land use types as the research object to study the soil infiltration process and its impact mechanism, in order to provide data support for the ecological restoration work in the wind erosion and water erosion transition zone.

The objectives of this study were to assess the changes in soil infiltrability in the water-wind erosion crisscross region of the Loess Plateau under cropland and grassland use, and to determine the key influencing factors for soil infiltrability changes based on soil properties and root system traits. Root morphological characteristics, soil physical properties and water infiltration were measured for three soil types under agricultural and grassland use. Specifically, we first investigated whether the different land uses affected soil physical properties and water infiltration. Then we examined the association between root traits, soil properties and infiltration rates. Finally, a conceptual pathway model (SEM) was proposed based on these results and previous studies. The proposed model (SEM) quantifies the specific contribution of soil properties to changes in soil infiltration capacity and provides a better understanding of the infiltration capacity response in different soils to different land use practices. This study proposed three hypotheses: (i) Converting cropland to grassland leads to better development of the soil's basic properties and infiltrability

in the water-wind erosion region. (ii) The infiltration capacity of the three soil types is inconsistent. (iii) Soil aggregates and soil organic matter are the two most important factors affecting soil infiltration.

2. Materials and Methods

2.1. Study Sites

The study was conducted in the Tragou sub-basin (39°34'~39°36' N, 110°54'~111°10' E) in Zhunger Banner, Ordos City, Inner Mongolia Autonomous Region, China. The watershed has a total area of 6.9 km² and an elevation of 800~1150 m, which belongs to the typical transition belt subjected to both water and wind erosion. It belongs to a mid-temperate continental monsoon climate, with an annual mean temperature of 8.8 °C to 10 °C. The average annual precipitation is about 400 mm, which is concentrated from July to September, accounting for 70~80% of the annual precipitation [34]. The average wind speed is about 3 m/s throughout the year, and the annual average of nearly 30 windy days is the main cause of wind erosion [35]. The main soil types in the basin are loess soils (WRB soil classification system) of loess parent material (USDA soil texture category, Table S1); wind-sand soils, generated by alluvial and wind-sand parent materials; and Pisha sandstone weathered soils, with a staggered distribution of the three soil types [36]. The study area is mainly covered by agricultural arable land and abandoned natural grassland, such as *Elymus dahuricus* Turcz., *Melilotus officinalis* (L.) Lam, *Caragana korshinskii* Kom, *Zea mays* L., *Stipa capillata* L., and *Lespedeza bicolor* Turcz. All of them were abandoned or cultivated for approximately 15 years.

2.2. Measurements of Soil Properties

The experimental measurements were mainly conducted in June–July 2021. The study site was located in sunny sloped fields in the Trach Gully watershed. In this study, one agricultural plot and one grassland plot were selected for the windy sandy soil, the Pisha sandstone soil, and the loess soil (Figure 1), and the grassland is formed by abandoning cropland for more than 15 years. Basic information for each sample plot is shown in Table 1. Three sampling points were randomly and evenly selected at equal intervals (5 m) for each sample plot, and 54 soil samples were collected in three layers from 0–30 cm of topsoil (5 cm in the middle of each layer) at 10 cm each by utilizing a 100 cm³ ring knife.

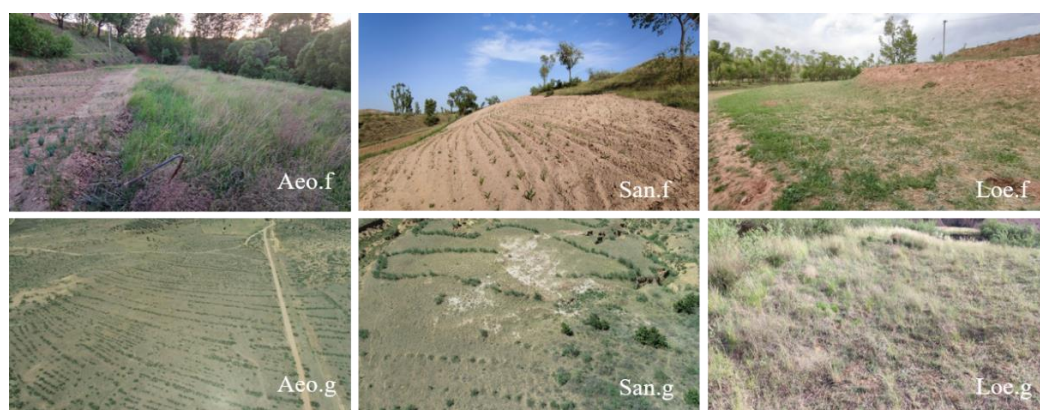


Figure 1. Sampling sites of the land-use types in the water-wind erosion crisscross region. Aeof, aeolian sandy soil cropland; Aeog, aeolian sandy soil grassland; San.f, Pisha sand soil cropland; San.g, Pisha sand soil grassland; Loe.f, loess soil cropland; Loe.g, loess soil grassland.

Determination of bulk density (BD), saturated moisture content (SMC), and calculation of total soil porosities (TP) was conducted using the drying weighing method [3]. Soil organic matter (SOM) was measured by the K₂Cr₂O₇-H₂SO₄ oxidation method [37]. The mechanical components of the soil was analyzed and determined using a Malvern laser particle size analyzer (MS 2000, MarvIn, UK). A complete soil core sample was collected

using a steel ring at three different soil layers: 0–10, 10–20, and 20–30 cm in depth. The plant roots were carefully separated from attached soil particles. Roots were washed and surface dried with absorbent paper. Finally, root images were taken by using the Epson Perfection V370 Photo Scanner (Seiko Epson Corporation, Nagano, Japan), preceded by the computer software Win-Rhizo, 2009, and the root diameter was measured (root length density, root area index) [38,39].

Table 1. Basic Information of Various Lands.

Plots	Community Component	Slope (°)	Coverage (%)	Altitude (m)
Aeo.f	<i>Zea mays</i> L. <i>Thymus mongolicus</i> Ronn. <i>Melilotus officinalis</i> (L.) Lam.	0~5	75~90	1160
Aeo.g	<i>Artemisia sacrorum</i> Ledeb. ex Hook.f. <i>Oxytropis bicolor</i> Bunge <i>Caragana korshinskii</i> Kom.	0~5	52~62	1080
San.f	<i>Zea mays</i> L. <i>Thymus mongolicus</i> Ronn. <i>Caragana korshinskii</i> Kom.	0~5	5~12	1130
San.g	<i>Artemisia sacrorum</i> Ledeb. ex Hook.f. <i>Stipa capillata</i> L.	0~5	32~43	1100
Loe.f	<i>Lespedeza bicolor</i> Turcz. <i>Medicago sativa</i> L. <i>Elymus dahuricus</i> Turcz.	0~5	65~74	1103
Loe.g	<i>Medicago sativa</i> L. <i>Artemisia sacrorum</i> Ledeb. ex Hook.f. <i>Scutellaria baicalensis</i> Georgi	0~5	40~51	1050

2.3. Measurements of Soil Aggregate Traits

The aggregates traits were determined using the wet-sieving method (DIK-2012 soil aggregate analyzer [40]). Take three random replicates from each plot to collect approximately 800 g of undisturbed soil ranging from 0 to 30 cm in layers every 10 cm by using an aluminum box. Take 500 g of air-dried soil samples, pass through sieve sets with apertures of 0.25, 0.5, 1, 2, and 5 mm, and sieve them for 12 min on Model 8411 Vibrating Sieve Apparatus (Shaoxing, China). Weigh to obtain the mass corresponding to each particle size aggregate. According to the mass percentages of each particle size obtained by dry sieving, 50 g of air-dried soil samples were prepared, then wet sieve for 60 s using an aggregate analyzer and water-stable aggregates of corresponding particle size were obtained. Finally, the percentage of water-stable aggregates was calculated by weighing the aggregates of each particle size after drying. Aggregate destruction rate (*PAD*), fractal dimension (*D*), aggregate mean weight diameter (*MWD*), and geometric mean diameter (*GMD*) were calculated as follows. Equations (1)–(6) were used as indicators for soil aggregates stability [41]:

$$w_i = W_i / W_T \times 100\% \quad (1)$$

$$W_{d>0.25} = 1 - W_{d>5} - W_{d<0.25} / W_T + W_{d>5} / W_T \quad (2)$$

$$MWD = \sum_{i=1}^n (\bar{d}_i w_i) / \sum_{i=1}^n w_i \quad (3)$$

$$GMD = \exp \left\{ \sum_{i=1}^n w_i \ln d_i \right\} \quad (4)$$

$$D = 3 - \left[\lg \frac{w(\delta \leq \bar{d}_i)}{w_T} / \lg \frac{\bar{d}_i}{d_{max}} \right] \quad (5)$$

$$PAD = \frac{M_d - M_w}{M_d} \times 100\% \quad (6)$$

where w_i is the percentage of the mass of the i -th level aggregate to the total mass of the aggregate. W_i is the mass of the i -th level water stable aggregate; W_T is the total mass of aggregates of each particle size. \bar{d}_i is the average diameter of the i -level aggregate; d_{max} is the maximum particle size of water-stable aggregates; $W_{(d < \bar{d}_i)}$ is the aggregate mass with a particle size smaller than \bar{d}_i ; $W_{d > 0.25}$ is the mass of aggregates with a particle size > 0.25 mm; M_d is the mass percentage of particle diameter > 0.25 mm after dry sieving of the sample (%); M_w is the mass percentage of the particle diameter > 0.25 mm after wet sieving of the sample; and $w_{(\delta \leq \bar{d}_i)}$ is the mass percentage of particles with particle size less than or equal to \bar{d}_i (%).

2.4. Measurements of Soil Infiltration Traits

The disc infiltration meter is widely used due to its ease of use and excellent suitability for a variety of soil infiltration applications [42–44]. The disc infiltration test of the sample plot in the study area was completed from 1–7 June 2021. The soil infiltration rate was measured following the method described by Zhu Liangjun et al. [45]. The soil porosities and infiltration rate of each sample were categorized and related calculations were done based on the measurement results [46–48]. Calculations for soil pore traits and disc infiltrability are as follows:

$$f_s = \frac{\Delta h D_2^2}{\Delta t D_1^2 (0.7 + 0.03T)} \quad (7)$$

$$\gamma = -\frac{2\sigma \cos \theta}{\rho g h} \approx -\frac{0.3}{h} \quad (8)$$

$$N = \frac{8\mu K_m}{\pi \rho g (r_m)^4} \quad (9)$$

$$\theta_m = N \pi r_m^2 = \frac{8\mu K_m}{\rho g (r_m)^2} \quad (10)$$

where f_s is the infiltration rate at 10 °C water temperature (mm/min); Δh is the water level difference (mm) in a certain measurement period Δt ; D_1 is the effective diameter of the infiltration disc (cm); D_2 is the diameter of the water storage pipe of the infiltrator (cm); Δt is the measurement period (min); T is the average water temperature during a certain measurement period (°C); γ is the equivalent pore (mm); σ is the water surface tension (g/s^2 , 74.2 at 10 °C); θ is the water-pore contact angle (°); ρ is the density of water (1.0 g/cm^3); g is the acceleration due to gravity (9.8 m/s^2); h is head pressure height (cm); N is the maximum number of effective pores per unit area (m^2); μ is the viscosity coefficient of water ($\text{g/m}\cdot\text{s}$); K_m is the tensile conductance of the largest pore (difference between two adjacent head pressures, m/s); and r_m is the minimum pore radius set (m); θ_m is the porosity (%).

The saturated hydraulic conductivity (SHC) determined by the ring knife method is the most commonly used index to reflect the vertical change of soil hydraulic properties [49]. The specific method was to randomly and evenly select 3 sampling points in different plots, using a 100 cm^3 ring knife to divide the 0–30 cm surface layer of undisturbed soil into 3 layers of 10 cm per layer (take the middle 5 cm of each layer), and used the constant water head method to measure the saturated hydraulic conductivity of the soil [50]. Experiments ran from 14–25 June 2021.

2.5. Statistical Analysis

Duncan's posthoc test was used to compare the differences in soil basic properties, root system traits, disc water infiltration rate, and saturated hydraulic conductivity of 0–30 cm soil profiles between different treatments. The relationship between water infiltration rate and disc infiltration time was fitted with the Kostikov model. In this study, the water infiltration process was divided into two phases based on changes in soil infiltration rates.

The initial infiltration stage was the first 10 min (AIR), and the stable infiltration stage was 10–30 min (SIR).

The direct and indirect effects of aggregates and the physical properties of soil on its infiltration capacity were evaluated using the partial least squares path model (SEM). For the SEM model to achieve a high level of statistical strength when other methods do not converge or offer acceptable solutions [27,51], it relies on a least squares regression with minimal sample size requirements. In this paper, Amos was applied to fit the SEM model, and the statistical analysis of the data was conducted using R 4.1.2, SPSS 22.0, and SPSS Amos 24 software.

3. Results

3.1. Soil Infiltration Rates under Different Land Use Patterns

3.1.1. Simulation Results of the Soil Infiltration Process

The Kostiakov model is one of the most commonly used models for studying infiltration. It uses empirical parameters to reflect the decreased degree of soil initial infiltration rate and steady infiltration rate over time, and better assess soil infiltration capacity comprehensively [52]. The grassland parameters (*a*, *b*) were higher than cropland parameters (*a*, *b*) (Table 2). This indicated returning cropland to grassland significantly improved the soil’s initial infiltration capacity (Figure 2). Compared with cropland, grassland had higher initial infiltration rates (AIR) and stable infiltration rates (SIR, Figure 3).

Table 2. Fitting parameters of soil infiltration model.

Fitting Parameters	Aeo.f	Aeo.g	San.f	San.g	Loe.f	Loe.g	
Kostiakov: $f(t) = at^{-b}$	<i>a</i>	3.9857	5.1254	4.3413	9.1090	2.2813	3.2108
	<i>b</i>	−0.2433	−0.3342	−0.2946	−0.2416	−0.3135	−0.3678
	<i>R</i> ²	0.8245	0.8517	0.7674	0.8064	0.7753	0.9141

Note: *f*(*t*) and *t* of the Kostiakov model are measured permeation rate and permeation time, respectively; *a* and *b* are empirical parameters without physical meaning. The value of *a* can reflect the initial infiltration rate of the soil, and the value of *b* indicates the degree of infiltration rate decrease with time. The value of *R*² reflects the model determination coefficients for the three soil types of cropland and grassland. Aeo.f, aeolian sandy soil cropland; Aeo.g, aeolian sandy soil grassland; San.f, Pisha sand soil cropland; San.g, Pisha sand soil grassland; Loe.f, loess soil cropland; Loe.g, loess soil grassland.

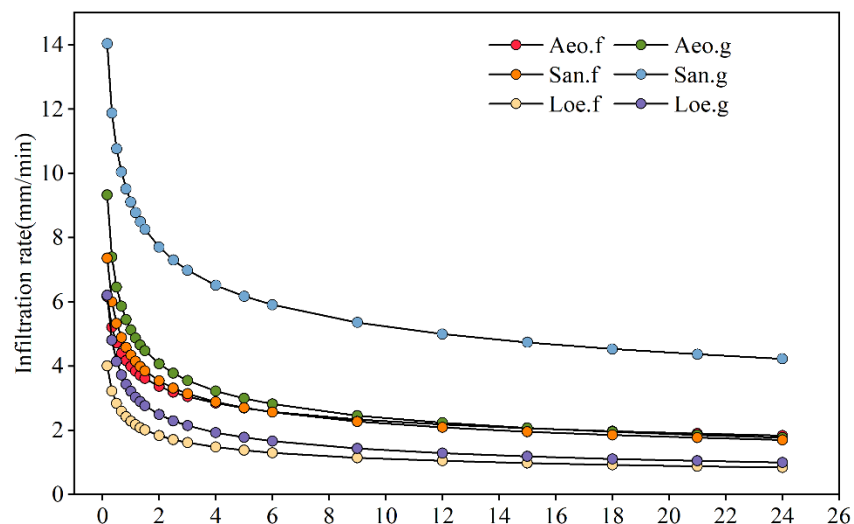


Figure 2. Soil moisture infiltration process of three types of soils in cropland and grassland. Aeo.f, aeolian sandy soil cropland; Aeo.g, aeolian sandy soil grassland; Loe.f, loess soil cropland; Loe.g, loess soil grassland; San.f, Pisha sand soil cropland; San.g, Pisha sand soil grassland.

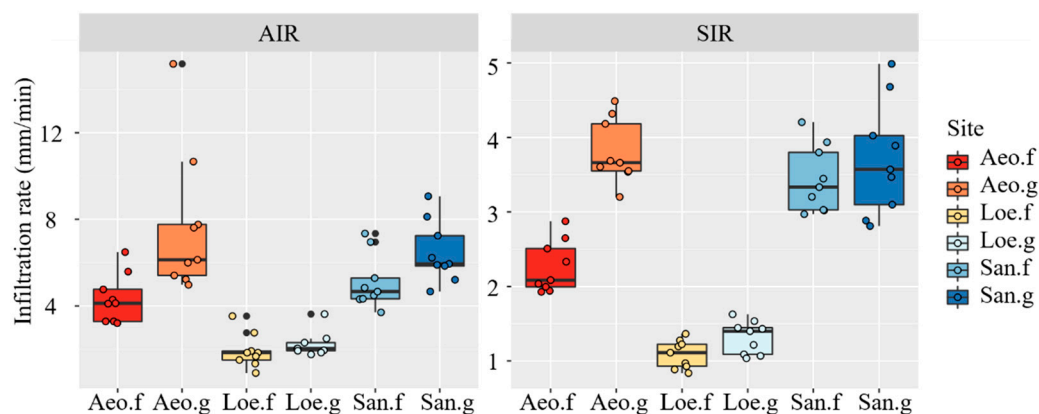


Figure 3. Comparison of initial infiltration rate AIR and steady infiltration rate SIR of three types of soil in cropland and grassland. Aeo.f, aeolian sandy soil cropland; Aeo.g, aeolian sandy soil grassland; Loe.f, loess soil cropland; Loe.g, loess soil grassland; San.f, Pisha sand soil cropland; San.g, Pisha sand soil grassland; AIR, initial infiltration state (0–10 min); SIR, steady infiltration state (10–30 min).

However, the difference between the loess soil infiltration rate under the two land use types was the smallest. Compared with cropland, grassland had a faster attenuation of aeolian sandy soil and loess soil, while Pisha sandstone soil was slower. San.g exhibited the two stages of the infiltration rate that was significantly higher than cropland (Figures 2 and 3). Furthermore, during the subsequent stable infiltration phase, this difference between the two land use types gradually became smaller. These results confirmed the cultivated land conversion increased soil infiltration capacity. The effect of Pisha sandstone soil was the best, followed by aeolian sandy soil and loess soil (Figures 2 and 3).

3.1.2. Changes in Soil-Saturated Hydraulic Conductivity

Compared with the double-ring method, the disc infiltration method (single-ring method) can cause major errors because of water-side infiltration, especially for Pisha sandstone soil infiltration with sheet structure [53]. To eliminate the error caused by lateral infiltration, ring knife sampling was conducted to measure the saturated infiltration rate on the three soil types.

The soil-saturated infiltration rate decreased rapidly with soil depth (Figure 4). The cropland saturated infiltration rate in the 0–10 cm soil layer was significantly higher than in grassland ($p < 0.05$). In contrast, the saturated infiltration rate had no significant difference between cropland and grassland of the three soil types in the 20–30 cm layer ($p > 0.05$). The infiltration capacity of aeolian sandy soil and loess soil grassland was significantly higher than that of cropland in the 10–20 cm soil layer (Figure 4). However, the SHC in san.g decreased which was significantly different among the measured disc infiltration meters. Specifically, excluding the influence of side infiltration, the infiltration capacity of Pisha sandstone soil in grassland was pronounced worse than that in cropland.

The SHC of sandy grassland was significantly better than that of cropland in the 0–20 cm layer ($p < 0.05$, Figure 4), which indicated that grassland vegetation may significantly improve the infiltration rate of aeolian sandy soil. In the 10–20 cm layer of loess soil, grassland was better than cropland, but there was no significant difference in the 20–30 cm layer ($p > 0.05$, Figure 4). Grassland had not yet reached this depth for the loess soil infiltration rate improvement. The infiltration capacity of San.f was higher than San.g. It demonstrated that even after removing lateral disc infiltration influence, the vertical void formation capacity of grassland root development cannot replace the tillage penetrating effect on the aquifer. As a whole, the saturation infiltration rate order had visibly shifted. Vertical infiltration rate was highest in loess soil, second in aeolian sandy soil, and lowest in Pisha sandstone soil.

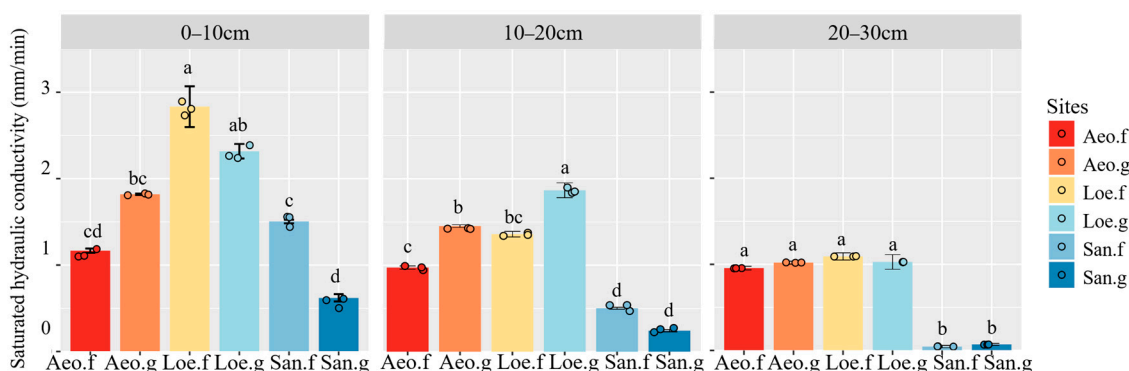


Figure 4. Comparison of saturated hydraulic conductivity (SHC) of three types of soil grassland and cropland; different lowercase letters indicate significant differences between different plots ($p < 0.05$). Aeo.f, aeolian sandy soil cropland; Aeo.g, aeolian sandy soil grassland; Loe.f, loess soil cropland; Loe.g, loess soil grassland; San.f, Pisha sand soil cropland; San.g, Pisha sand soil grassland.

3.2. Soil Properties under Different Land Uses

3.2.1. Physical Properties of Three Soil Types

The SOM, RLD, and RAI of grassland were significantly higher than those of cropland ($p < 0.05$, Table 3), while BD, SMC, and TP were lower than those of cropland. The performance of the aeolian sandy soil and Pisha sandstone soil grassland was worse than that of the cropland, except the BD, SMC, and TP of the Loe.g were all higher than those of Loe.f.

Table 3. Comparison of the mean value (mean \pm standard deviation) of soil basic physical properties during the process of cropland returning to grassland.

Plots	Depth (cm)	BD (g/cm ³)	SOM (g·kg ⁻¹)	WSA (%)	SMC (%)	TP (%)	RLD (m/m ³)	RAI (m ² /m ³)
Aeo.f	0–10	1.33 \pm 0.09 b	6.09 \pm 0.51 Ad	34.19 \pm 1.70 Ae	37.72 \pm 1.96 Ab	49.99 \pm 3.41 a	30.47 \pm 3.4 Ad	125.65 \pm 10.30 Ad
	10–20	1.36 \pm 0.03 c	3.13 \pm 0.37 Bd	29.15 \pm 1.38 Bd	36.04 \pm 1.86 Aab	48.69 \pm 3.43 a	25.52 \pm 1.98 Bd	59.75 \pm 7.56 Bd
	20–30	1.43 \pm 0.03 cd	2.88 \pm 0.15 Cd	32.35 \pm 0.92 Ad	32.13 \pm 1.40 Ba	45.97 \pm 1.09 a	21.75 \pm 2.71 Cc	36.03 \pm 4.65 Cd
Aeo.g	0–10	1.50 \pm 0.09 Ca	7.10 \pm 0.15 Ac	26.72 \pm 0.79 BCf	28.98 \pm 1.93 Ac	43.44 \pm 1.52 Ab	31.71 \pm 5.93 Bd	67.57 \pm 7.56 Ce
	10–20	1.58 \pm 0.02 BCb	4.86 \pm 0.30 Bd	25.06 \pm 0.71 Ce	25.69 \pm 0.77 Bc	40.50 \pm 0.72 Bb	39.68 \pm 4.11 Ac	128.15 \pm 10.09 Ab
	20–30	1.61 \pm 0.02 Ab	2.65 \pm 0.12 Cc	27.69 \pm 1.14 Ae	24.33 \pm 0.79 Bbc	39.19 \pm 0.77 Bc	31.95 \pm 2.47 Ba	78.18 \pm 8.03 Ba
San.f	0–10	1.32 \pm 0.05 Bb	7.15 \pm 0.24 Ac	39.20 \pm 1.16 Bd	38.23 \pm 2.62 Ab	50.29 \pm 1.73 Aa	8.81 \pm 1.63 Ae	17.11 \pm 2.01 Af
	10–20	1.71 \pm 0.07 Aa	3.98 \pm 0.30 Bd	52.50 \pm 1.29 Ac	21.53 \pm 0.15 Bd	35.56 \pm 0.98 Bc	1.88 \pm 0.24 Bf	4.15 \pm 1.04 Bf
	20–30	1.72 \pm 0.08 Aa	3.62 \pm 0.39 Bc	48.91 \pm 3.31 Ac	20.39 \pm 2.86 Bcd	30.41 \pm 1.55 Cd	1.71 \pm 0.17 Be	4.08 \pm 1.01 Bf
San.g	0–10	1.59 \pm 0.08 Ca	8.41 \pm 0.38 Ab	59.58 \pm 0.44 Ba	26.08 \pm 1.50 Ac	40.13 \pm 1.84 Ab	54.50 \pm 6.06 Ac	145.54 \pm 15.92 Ac
	10–20	1.75 \pm 0.07 Aa	4.28 \pm 0.24 Bc	67.26 \pm 0.77 Aa	20.45 \pm 0.60 Bd	34.51 \pm 0.52 Bc	10.71 \pm 3.32 Be	10.16 \pm 2.31 Be
	20–30	1.71 \pm 0.05 BCa	4.17 \pm 0.30 Cb	64.94 \pm 2.37 Aa	17.63 \pm 0.87 Cd	31.84 \pm 0.91 Cd	4.13 \pm 0.91 Cd	8.74 \pm 1.05 Be
Loe.f	0–10	1.32 \pm 0.05 b	9.59 \pm 0.25 Aa	56.50 \pm 1.48 b	38.34 \pm 0.62 Ab	50.31 \pm 1.68 a	74.75 \pm 5.06 Ab	146.54 \pm 12.91 Ab
	10–20	1.39 \pm 0.04 c	5.91 \pm 0.30 Bb	58.69 \pm 2.69 b	34.56 \pm 2.23 BCb	47.77 \pm 1.59 a	46.81 \pm 5.53 Bb	86.95 \pm 18.31 Bc
	20–30	1.41 \pm 0.06 d	5.86 \pm 0.26 Cb	59.61 \pm 2.54 b	32.20 \pm 4.20 Ca	45.91 \pm 3.25 a	20.13 \pm 2.23 Cc	41.24 \pm 11.24 Cc
Loe.g	0–10	1.24 \pm 0.04 Cb	10.06 \pm 0.17 Aa	53.84 \pm 1.89 Ac	43.19 \pm 0.93 Aa	53.28 \pm 1.62 Aa	89.65 \pm 13.05 Aa	202.18 \pm 28.32 Aa
	10–20	1.32 \pm 0.01 Bc	7.81 \pm 0.36 Ba	23.16 \pm 1.27 Ce	38.27 \pm 0.23 Ba	50.35 \pm 0.15 Ba	56.14 \pm 8.87 Ba	135.34 \pm 22.13 Ba
	20–30	1.51 \pm 0.04 Ac	5.37 \pm 0.47 Ca	28.76 \pm 3.18 Bde	28.20 \pm 1.68 Cab	42.50 \pm 1.85 Cb	27.66 \pm 7.98 Cb	63.29 \pm 11.40 Cab

In addition, the soil organic matter (SOM) decreased with the soil layer depth of three soil types in the 0–30 cm soil layer. The RLD and RAI followed by loess soil > aeolian sand soil > Pisha sandstone soil (Table 3), and decreased rapidly with increasing soil depth. Different capital letters indicate significant differences ($p < 0.05$) between the different soil depths for the same land by ANOVA. Different lowercase letters indicate significant differences ($p < 0.05$) between the different land for the same soil depth.

3.2.2. Aggregate Structures of Three Soil Types

The micro-aggregates and macro-aggregates (>0.25 mm) of the content in 0–10 cm grassland were higher than those of cropland (Figure 5), which indicated that the soil aggregate structure of surface grassland was better than that of cropland. The micro-aggregate content increased rapidly by 10–30 cm in Loe.g (Figure 5). Therefore, the aggregate structure was worse than that of cropland. In contrast, the macro-aggregates and micro-aggregates content in San.g is also lower than San.f. Although the micro-aggregate

content in Ae0.g was higher than that in Ae0.f, the aggregate content with other particle sizes was too low. Specifically, the soil aggregate structure of middle and lower grassland was lower than that of cropland.

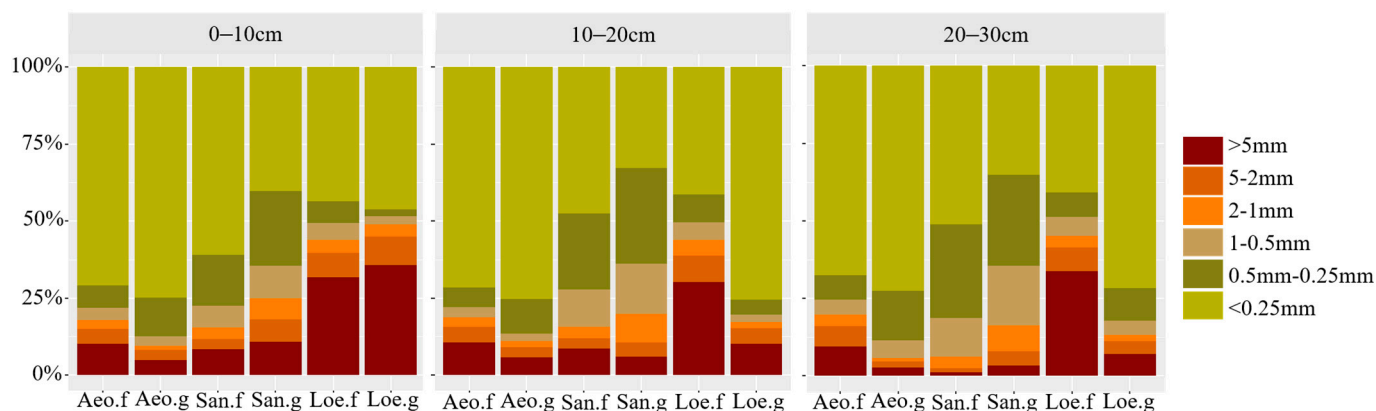


Figure 5. Aggregate structure for various particle sizes across three different types of cropland and grassland. Ae0.f, aeolian sandy soil cropland; Ae0.g, aeolian sandy soil grassland; Loe.f, loess soil cropland; Loe.g, loess soil grassland; San.f, Pisha sand soil cropland; San.g, Pisha sand soil grassland.

The aggregate structure of aeolian soil hardly changed with soil depth. In the 0–10 cm soil layer, the macro-aggregate content (>5 mm) of the Loe.g was 35.70% and the micro-aggregate content was 46.16%. Therefore, the soil aggregate structure was the best among the three depths (Figures 5 and S1). The macro-aggregates and micro-aggregates content in the Pisha sandstone soil still decreased with soil depth. The performance order of the soil aggregate structure followed by loess soil > Pisha sandstone soil > aeolian sandy soil (Figures 5 and S1).

3.3. Relationships between Root Traits, Soil Properties, and Soil Infiltration Capacity

Root traits were significantly positively correlated with SHC ($p < 0.01$, Table 4), but not significantly positively correlated with AIR and SIR ($p > 0.05$, Table 4). GMD was not significantly positively correlated with SHC ($p > 0.05$, Table 4), but was significantly correlated with AIR and SIR ($p < 0.05$, Table 4). In soil texture, sand was significantly negatively correlated with MWD, GMD, AIR (MWD $p < 0.01$, GMD $p < 0.01$, AIR $p < 0.05$, Table 4), and SIR ($p < 0.05$, Table 4), but silt and clay were significantly positively correlated with MWD, GMD, AIR, and SIR ($p < 0.05$, $p < 0.01$, Table 4). But soil texture was not significantly correlated with SHC ($p > 0.05$, Table 4). Both aggregates and root systems were positively correlated, which was especially evident for RLD.

3.4. Path Modeling of the Effects of Soil Properties on Soil Water Infiltration

Because disc infiltration was affected by horizontal water infiltration [54], this study selected saturated indoor soil hydraulic conductivity to represent the soil vertical infiltration, and combined factors with good correlation in the correlation analysis results in Table 4 to establish a structural equation model (SEM) for analysis.

The model explained 65% of the variance in saturated hydraulic conductivity (SHC). SOM, TP, and MWD directly affected water infiltration. Soil porosity had a significant positive effect on saturated hydraulic conductivity (SHC, $p < 0.05$), and the contribution of organic matter to saturated hydraulic conductivity (SHC) was also dominated by direct effects (Figure 6a,b). Moreover, the cross-loading effects representing differentiation between different soil textures indicated that the direct contribution to saturated hydraulic conductivity (SHC) was not significant (standardized path coefficient of 0.23, $p > 0.05$); it still exhibited a significant effect on soil aggregates ($p < 0.05$, Figure 6).

Table 4. Pearson correlations for between soil texture, root morphological traits, soil properties and soil infiltration rates.

	BD	WSA	SOM	SMC	TP	Clay	Silt	Sand	D	GMD	MWD	PAD	RLD	RAI	SHC	AIR	SIR
BD	1	0.283	−0.558 *	−0.989 **	−0.984 **	−0.214	−0.205	0.297	0.314	−0.407	−0.551 *	−0.065	−0.621 **	−0.586 *	−0.673 **	−0.362	−0.539 *
WSA		1	0.254	−0.253	−0.303	0.522 *	0.608 **	−0.488 *	−0.449	0.665 **	0.519 *	−0.891 **	−0.036	−0.159	−0.164	0.140	0.038
SOM			1	0.596 **	0.567 *	0.118	0.248	−0.241	−0.480 *	0.602 **	0.594 **	−0.157	0.759 **	0.694 **	0.754 **	0.030	0.172
SMC				1	0.983 **	0.176	0.178	−0.270	−0.373	0.420	0.560 *	0.044	0.648 **	0.611 **	0.386	0.349	0.504 *
TP					1	0.158	0.149	−0.245	−0.300	0.388	0.540 *	0.083	0.643 **	0.612 **	0.707 **	0.309	0.484 *
Clay						1	0.959 **	−0.975 **	−0.261	0.571 *	0.559 *	−0.610 **	−0.026	−0.199	−0.042	0.521 *	0.484 *
Slit							1	−0.974 **	−0.355	0.688 **	0.648 **	−0.615 **	0.078	−0.123	0.032	0.605 **	0.563 *
Sand								1	0.283	−0.646 **	−0.644 **	0.536 *	−0.100	0.085	−0.086	−0.589 *	−0.557 *
D									1	−0.565 *	−0.526 *	0.453	−0.427	−0.372	−0.198	0.267	0.238
GMD										1	0.975 **	−0.690 **	0.541 *	0.381	0.466	0.505 *	0.569 *
MWD											1	−0.603 **	0.580 *	0.429	0.536 *	0.517 *	605 **
PAD												1	0.000	0.116	0.096	−0.230	−0.188
RLD													1	0.945 **	0.928 **	0.208	0.358
RAI														1	0.862 **	0.093	0.233
SHC															1	−0.104	−0.332
AIR																1	0.918 **
SIR																	1

Note: Spearman correlations for root traits, soil physical properties and infiltration rates. BD: bulk density, WSA: water-stable Aggregates; SOM: organic matter, SMC: saturated soil moisture content, TP: total porosity; Sand: sand; Silt: silt; Clay: clay; D: fractal dimension; GMD: geometric mean diameter; MWD: aggregate mean weight diameter; PAD: Aggregate destruction rate; RLD: root length density, RAI: root surface area density; SHC: saturated hydraulic conductivity; AIR: initial infiltration state (0–10 min); SIR: steady infiltration state (10–30 min). The significance levels: * $p < 0.05$, ** $p < 0.01$.

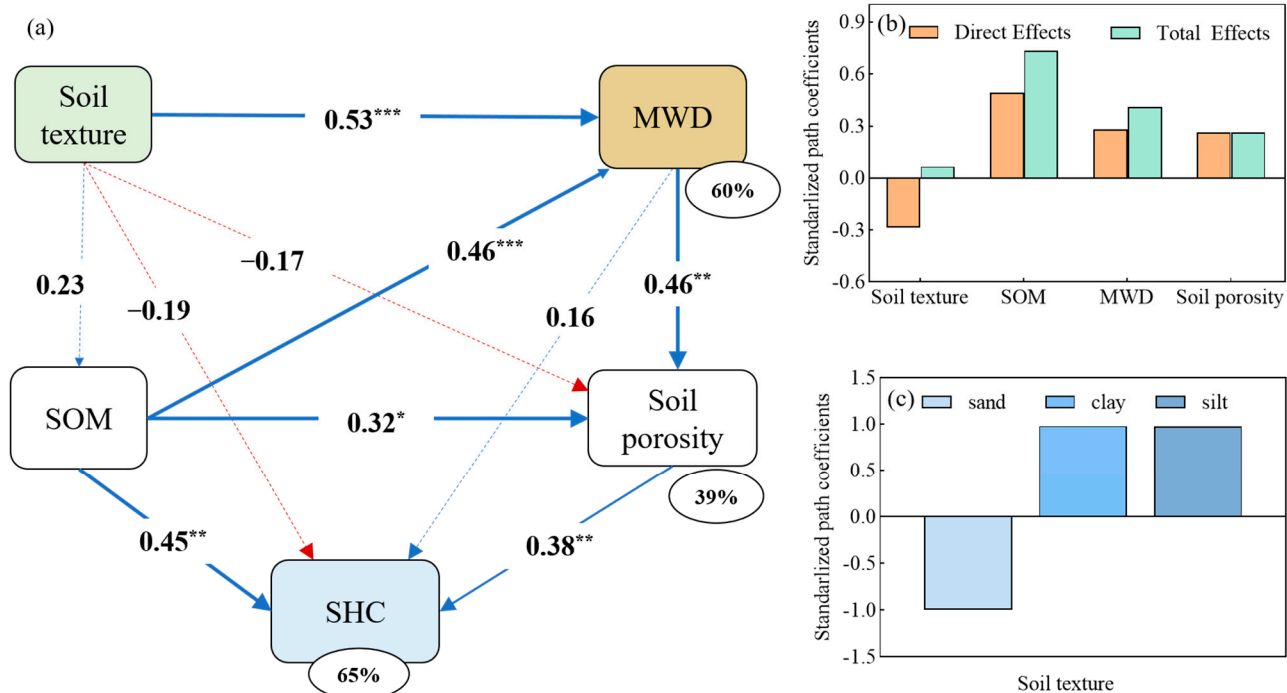


Figure 6. Effects of soil texture (clay, silt, sand), soil organic matter, average weight diameter of soil aggregates, and soil porosity on SHC determined by the ring knife method: (a) SEM output: Numbers on arrows are normalized path coefficients; blue arrows are positive, and red arrows are negative. Bold and solid arrows indicate significant standardized path coefficients (significance level is *, $p < 0.05$, ** indicates $p < 0.01$, *** indicates $p < 0.001$), thin and dotted arrows indicate non-significant standardized path coefficients ($p > 0.05$). The percentage near the circle indicates the variance R^2 explained by the model, and the goodness-of-fit for the model is 0.99; (b) Normalized path coefficients for the direct and total effects of soil texture, organic matter, MWD, and soil porosity on stable infiltration rates; (c) Path model cross-sectional effect of soil texture (clay, silt, sand) on the steady infiltration rate of soil moisture.

4. Discussion

The overall change of infiltration curves law was consistent with some previous studies in the Loess Plateau hilly gully area and water-wind erosion crisscross region [55]. Land use can cause significant changes in soil texture, soil physical properties, and root morphological traits, which have been widely accepted to affect soil infiltration capacity via different pathways [56–60]. Our study found a positive impact on soil physical properties after a short period of returning cropland, such as the reduced soil bulk density, increased saturated water content, and root length density (Table 3, Figures 3 and 4) in the 0–20 cm soil layer. Compared with cropland, the root length density (RLD) and root area index (RAI) of Ae.o.g and Loe.g also increased significantly in the 0–20 cm soil layer (Table 3). Similarly, previous studies suggested that plant root density and complexity may improve soil physicochemical properties [10]. During the decomposition, plant roots form more preferred root channels in the upper soil layer than in the lower soil layer, thereby increasing soil porosities and organic matter in the surface soil and improving soil infiltration rates [21,61]. Moreover, our study revealed that root distribution was significantly correlated with soil infiltration (Figure 6). This may be due to the fact that root growth significantly increased soil organic matter, MWD, and soil porosities, which play important roles in regulating soil infiltration [27,30,62]. Long-term persistence in returning cropland to grassland affects soil properties, resulting in spatial variability in soil infiltration capacity.

The grassland infiltration rate was slightly higher than that of crop land, which may be due to the high content of aggregates >5 mm in the surface layer of loess soil grassland

(0–10 cm soil layer) (Figures 5 and S1, Table 4), the better characteristics of the plant root system, and the higher content of organic matter (Table 3)—which resulted in the best top layer of the soil agglomerates in the grassland and a low rate of damage to the top layer of the agglomerated structure under the combined effect (Figure S1). The D value of the loess soil grassland surface layer was significantly ($p < 0.05$) lower than that of several other sample plots (Figure S1, Table 4), indicating that the surface aggregate structure of the loess soil grassland was optimal, the aggregates were more stable, and the soil erosion resistance was also stronger [63]. In the second stage, there is no difference between grassland infiltration rate and cropland because the root length density and root surface area density of loess grassland were higher at 0–20 cm and slightly lower at 20–30 cm than in cropland. A large amount of alfalfa (Table 1) grew in the yellow cotton soil cropland, mycorrhizae were formed in the soil, and there were relatively thick root systems below 20 cm. Moreover, the 0.25–0.5 mm particle size aggregates in cropland were higher than those in grassland (Figure 5). Because the yellow cotton soil cropland was cultivated at a depth of about 30 cm before returning to cropland, the content of deep soil aggregates and mechanical composition was relatively balanced when returning to cropland, plant growth, and root system. It is also relatively more comprehensive during activities [64]. The content of >5 mm aggregates and micro-aggregates in the loess soil layers and grassland surface soil is relatively high (Figure 5), and the gradient is “V” in size, which was consistent with Su Jing and Zhao Shiwei [65]. It was consistent with the research results of Cheng et al. [66] in the southern Ningxia area of the Loess Plateau. In loess soil, the stability of soil aggregates was better in each layer. The similar rate in the second stage may also be due to the existence of a soil layer in the loess capable of generating a certain degree of water repellency [67–70], resulting in a short-term obstruction to infiltration of the wetting front during this period.

Soil texture had an indirect impact on saturated hydraulic conductivity (SHC) through its effect on soil aggregates and soil organic matter, with the largest standardized indirect effect being 0.53 (Figure 6a,b) and the most important silt content (Figure 6c). Soil organic matter, MWD, and total soil porosities are the main direct factors affecting hydraulic conductivity (Figure 6a,b). The soil organic matter path coefficient indirectly affecting aggregates is 0.46 (Figure 6a), and aggregate MWD has a positive contribution to soil hydraulic conductivity (SHC) by indirectly increasing soil porosity (Figure 6a). SOM has direct and indirect effects on soil infiltration (Figure 6a,b), and the direct effects come from providing energy and nutrients to soil organisms [71–74]. Indirect effects can be attributed to its induction of macro-aggregate formation and increased aggregate stability [75–80]. Soil aggregates either positively or negatively affect soil infiltration [21,27]. The MWD of aggregates had an indirect positive contribution to soil water infiltration by increasing soil porosity (Figure 6a), some previous studies also supported this [27,81,82]. As the primary route for water infiltration, soil porosity had a positive impact on soil infiltrability, which is in line with previous research [83].

The loess soil's saturated hydraulic conductivity (SHC) was higher than that of aeolian sandy soil and Pisha sandstone soil, which can be explained by the highest organic matter content, saturated water content, total porosity, root length density, and root area index of Loess (Table 3, [15,84], and the aggregates' structure and stability of loess soil are relatively the best (Figure S1 and Figure 5, [85,86]. Three possible reasons for the low saturated hydraulic conductivity of the Pisha sandstone soil can be cited. First, the Pisha rock soil must undergo a long period of collapse and expand to fully absorb water [87]. The second is that the Pisha sandstone soil exhibited stratification phenomena. The pores between layers are more permeable to water, while the inner layers are tightly packed and impermeable [88]. It gets denser when it is wet. In addition, Pisha sandstone soil has a low capacity for vertical infiltration. We dug up the contaminated Pisha sandstone soil to see that when the field disc penetrated, water flowed through the surface soil, and then vertical infiltration was greatly reduced, and it turned out to penetrate along the soil layer gap. Since vertical gaps in grassland root development are not a good replacement for farming, vertical gaps created by farming methods may gradually decrease after aban-

donment [89]. As root system characteristics (root length density, root area index) rapidly decrease in the middle and lower layers of Pisha sandstone soil, the aggregate structure also deteriorates (Tables 3 and 4, Figure 5) [3,85]. Different infiltration measurements reflect the mechanism difference between disc infiltration and ring knife technique. Therefore, both lateral infiltration and vertical infiltration of disc infiltration are mixed. It is necessary to wait for the Pisha sandstone soil to absorb and saturate. Its SHC was much lower than the disc infiltration rate because it also hinders vertical infiltration after lateral infiltration is removed.

Soil water conservation capacity and soil structure can be improved after 15 years of continuous conversion of cropland to grassland in the water-wind erosion crisscross region of the Loess Plateau, which is consistent with previous research conclusions [90]. According to the results of this research, crack flow and lateral flow can occur when water penetrates Pisha sandstone soil, and the lack of vertical infiltration capacity is a contributing factor to severe soil erosion in the area. Therefore, the water conductivity of Pisha sandstone soil decreases [21,91]. Most previous research has not taken into account quantifying the quantitative link between saturated hydraulic conductivity and vegetation properties, especially root characteristics [54,90,91], and further research in this area may be conducted.

5. Conclusions

In conclusion, our research results showed that the basic properties and infiltration capacity of the soil in the water-wind erosion criss-cross area of the Loess Plateau after cropland was converted to grassland for a period of time. The basic properties and infiltration capacity of the soil were improved, and the infiltration capacity of arsenic sandstone soil was only improved in the 0–10 cm surface layer. Loess soil had the highest increase in organic matter content (32.14%), the best aggregate structure, and the highest soil infiltration rate (43.6%). The organic matter in aeolian soil increased significantly in the three soil layers ($p < 0.05$), and the saturated hydraulic conductivity increased the most (33.7%). The reasons for the optimal infiltration rate and the worst saturated infiltration capacity of the arsenic sandstone soil disk were related to the loss of soil moisture in the horizontal direction and the insufficient vertical infiltration capacity. The research results helped to clarify that the improvement effect of grassland on the three types of soil in the water-wind erosion crisscross zone of the Loess Plateau was currently mainly in the shallow layer (within 20 cm), and the ability to restore deep soil infiltration remains to be studied. Secondly, improving the vertical infiltration performance of arsenic sandstone soil can play a positive role in local water and soil protection.

Supplementary Materials: The following supporting information can be downloaded at: <https://www.mdpi.com/article/10.3390/land12081485/s1>, Table S1: Soil mechanical composition of plots; Table S2: The references of proposed mechanisms for each pathway associated with the model; Figure S1: Characteristics of soil aggregates in various lands; Figure S2: A structural equation modeling (SEM) of the possible pathways of these key factors on soil infiltrability during the ecological restoration.

Author Contributions: Conceptualization, X.X.; methodology, X.X.; Software, X.R.; Validation, X.X.; Formal analysis, X.R.; Investigation, X.C., Y.Q., Y.X., F.U.K., J.W., P.G., W.W., Q.Z. and Q.W.; Resources, X.C., Y.Q., Y.X., F.U.K., P.G., W.W. and F.D.; Writing—original draft, X.R.; Writing—review & editing, X.R., X.C., Y.Q., J.W., X.X. and F.D.; Visualization, X.R.; Supervision, X.X.; Project administration, X.X.; Funding acquisition, X.X. All authors have read and agreed to the published version of the manuscript.

Funding: This research was supported by the National Natural Science Foundation of China (Grant No. 41977426, 41771322).

Data Availability Statement: We do not provide public access to the dataset due to protection of the privacy of participants. Regarding the details of the data, please contact the corresponding author.

Conflicts of Interest: The authors declare no conflict of interest.

References

- Schwärzel, K.; Zhang, L.; Montanarella, L.; Wang, Y.; Sun, G. How afforestation affects the water cycle in drylands: A process-based comparative analysis. *Glob. Chang. Biol.* **2020**, *26*, 944–959. [\[CrossRef\]](#)
- Zhao, G.; Mu, X.; Wen, Z.; Wang, F.; Gao, P. Soil erosion, conservation, and eco-environment changes in the Loess Plateau of China. *Land Degrad. Dev.* **2013**, *24*, 499–510. [\[CrossRef\]](#)
- Zhu, P.; Zhang, G.; Wang, H.; Xing, S. Soil infiltration properties affected by typical plant communities on steep gully slopes on the Loess Plateau of China. *J. Hydrol.* **2020**, *590*, 125535. [\[CrossRef\]](#)
- Zhang, C.; Wang, Y.; Shao, M. Controlling gully- and revegetation-induced dried soil layers across a slope–gully system. *Sci. Total. Environ.* **2021**, *755*, 142444. [\[CrossRef\]](#)
- Zhu, P.; Zhang, G.; Wang, H.; Zhang, B.; Liu, Y. Soil moisture variations in response to precipitation properties and plant communities on steep gully slope on the Loess Plateau. *Agric. Water Manag.* **2021**, *256*, 107086. [\[CrossRef\]](#)
- Wang, X.-P.; Cui, Y.; Pan, Y.-X.; Li, X.-R.; Yu, Z.; Young, M. Effects of rainfall characteristics on infiltration and redistribution patterns in revegetation-stabilized desert ecosystems. *J. Hydrol.* **2008**, *358*, 134–143. [\[CrossRef\]](#)
- Eldridge, D.J.; Wang, L.; Ruiz-Colmenero, M. Shrub encroachment alters the spatial patterns of infiltration. *Ecolhydrology* **2015**, *8*, 83–93. [\[CrossRef\]](#)
- Shi, X.; Qin, T.; Yan, D.; Tian, F.; Wang, H. A meta-analysis on effects of root development on soil hydraulic properties. *Geoderma* **2021**, *403*, 115363. [\[CrossRef\]](#)
- Bodner, G.; Leitner, D.; Kaul, H.-P. Coarse and fine root plants affect pore size distributions differently. *Plant Soil* **2014**, *380*, 133–151. [\[CrossRef\]](#)
- Leung, A.K.; Garg, A.; Coo, J.L.; Ng, C.W.W.; Hau, B.C.H. Effects of the roots of *Cynodon dactylon* and *Schefflera heptaphylla* on water infiltration rate and soil hydraulic conductivity. *Hydrol. Process.* **2015**, *29*, 3342–3354. [\[CrossRef\]](#)
- Korkanç, S.Y. Effects of the land use/cover on the surface runoff and soil loss in the Niğde-Akkaya Dam Watershed, Turkey. *Catena* **2018**, *163*, 233–243. [\[CrossRef\]](#)
- Cui, Z.; Wu, G.-L.; Huang, Z.; Liu, Y. Fine roots determine soil infiltration potential than soil water content in semi-arid grassland soils. *J. Hydrol.* **2019**, *578*, 124023. [\[CrossRef\]](#)
- Liu, Y.; Guo, L.; Huang, Z.; López-Vicente, M.; Wu, G.-L. Root morphological characteristics and soil water infiltration capacity in semi-arid artificial grassland soils. *Agric. Water Manag.* **2020**, *235*, 106153. [\[CrossRef\]](#)
- Wu, G.-L.; Cui, Z.; Huang, Z. Contribution of root decay process on soil infiltration capacity and soil water replenishment of planted forestland in semi-arid regions. *Geoderma* **2021**, *404*, 115289. [\[CrossRef\]](#)
- Ge, N.; Wei, X.; Wang, X.; Liu, X.; Shao, M.; Jia, X.; Li, X.; Zhang, Q. Soil texture determines the distribution of aggregate-associated carbon, nitrogen and phosphorous under two contrasting land use types in the Loess Plateau. *Catena* **2019**, *172*, 148–157. [\[CrossRef\]](#)
- Schweizer, S.A.; Bucka, F.B.; Graf-Rosenfellner, M.; Kögel-Knabner, I. Soil microaggregate size composition and organic matter distribution as affected by clay content. *Geoderma* **2019**, *355*, 113901. [\[CrossRef\]](#)
- Wang, Z.; Peng, R.; Wang, L.; Liu, L. Studies on Soil Properties of Aeolian Sandy Land Improvement and Utilization in South Edge of Musu Desert. *J. Soil Water Conserv.* **2006**, *20*, 14–21. [\[CrossRef\]](#)
- Bi, C.; Wang, F.; Li, G.; Qing, B.; Qiao, W.; Li, G. Experiment on sediment retention by plant “flexible dam” in gully in soft rock region. *J. Sediment Res.* **2003**, *2*, 14–25. [\[CrossRef\]](#)
- Han, J.; Liu, Y.; Luo, L. Research on the core technology of remixing soil by soft rock and sand in the Maowusu sand land region. *China Land Sci.* **2012**, *26*, 87–94. [\[CrossRef\]](#)
- Huang, Z.; Tian, F.; Wu, G.; Liu, Y.; Dang, Z. Legume Grasslands Promote Precipitation Infiltration better than Gramineous Grasslands in arid Regions. *Land Degrad. Dev.* **2017**, *28*, 309–316. [\[CrossRef\]](#)
- Lu, J.; Zhang, Q.; Werner, A.D.; Li, Y.; Jiang, S.; Tan, Z. Root-induced changes of soil hydraulic properties—A review. *J. Hydrol.* **2020**, *589*, 125203. [\[CrossRef\]](#)
- Elliott, J.A.; Efetha, A.A. Influence of tillage and cropping system on soil organic matter, structure and infiltration in a rolling landscape. *Can. J. Soil Sci.* **1999**, *79*, 457–463. [\[CrossRef\]](#)
- Abu-Hamdeh, N.H.; Abo-Qudais, S.A.; Othman, A.M. Effect of soil aggregate size on infiltration and erosion characteristics. *Eur. J. Soil Sci.* **2006**, *57*, 609–616. [\[CrossRef\]](#)
- Alaoui, A. Modelling susceptibility of grassland soil to macropore flow. *J. Hydrol.* **2015**, *525*, 536–546. [\[CrossRef\]](#)
- Liu, Y.-F.; Zhang, Z.; Liu, Y.; Cui, Z.; Leite, P.A.; Shi, J.; Wang, Y.; Wu, G.-L. Shrub encroachment enhances the infiltration capacity of alpine meadows by changing the community composition and soil conditions. *Catena* **2022**, *213*, 106222. [\[CrossRef\]](#)
- Hao, H.-X.; Wei, Y.-J.; Cao, D.-N.; Guo, Z.-L.; Shi, Z.-H. Vegetation restoration and fine roots promote soil infiltrability in heavy-textured soils. *Soil Tillage Res.* **2020**, *198*, 104542. [\[CrossRef\]](#)
- Fayos, C.B. The roles of texture and structure in the water retention capacity of burnt Mediterranean soils with varying rainfall. *Catena* **1997**, *31*, 219–236. [\[CrossRef\]](#)
- Nyamangara, J.; Gotosa, J.; Mpfu, S. Cattle manure effects on structural stability and water retention capacity of a granitic sandy soil in Zimbabwe. *Soil Tillage Res.* **2001**, *62*, 157–162. [\[CrossRef\]](#)
- Wang, P.; Su, X.; Zhou, Z.; Wang, N.; Liu, J.; Zhu, B. Differential effects of soil texture and root traits on the spatial variability of soil infiltrability under natural revegetation in the Loess Plateau of China. *Catena* **2023**, *220*, 106693. [\[CrossRef\]](#)

30. Xiang, L.; Zeng, L.; Yuan, Y. Key Laboratory of eco-environments in three gorges reservoir region (Ministry of Education). *Lab. Nat. Prod. POJ* **2012**, *5*, 503–507.
31. Liu, K.; Wang, L.; Song, N.P.; Yang, X.Y.; Chen, L. Soil infiltration characteristics of Caragana korshinkii plantation with different ages in south edge of Mu Us Sandy Land. *J. Arid. Land Resour. Environ.* **2013**, *27*, 89–94. [[CrossRef](#)]
32. Yang, Z.Q.; Qin, F.C.; Li, M.Y.; Li, L.; Qian, Q.Y.; Li, Y. Soil infiltration capacity and its influencing factors of different land use types in feldspathic sandstone region. *Ecol. Environ. Sci.* **2020**, *29*, 733–739. [[CrossRef](#)]
33. Zhao, G.; Mu, X.; Wen, Z.; Wang, F.; Gao, P. Impacts of precipitation and human activities on streamflow and sediment load in the Huangfuchuan Watershed. *Sci. Soil Water Conserv.* **2013**, *11*, 1–8. [[CrossRef](#)]
34. Yan, F.C.; Jiao, J.Y.; Cao, B.T.; Yu, W.J.; Wei, Y.; Kou, M.; Hu, S. Soil anti-erodibility of abandoned lands during different succession stages of plant community in hilly-gullied region of the Loess Plateau: Take Fangta small watershed as an example. *Yingyong Shengtai Xuebao* **2016**, *27*, 64–72. [[CrossRef](#)]
35. Shahid, S.A.; Abdelfattah, M.A.; Wilson, M.A.; Kelley, J.A.; Chiaretti, J.V. *United Arab Emirates Keys to Soil Taxonomy*; Springer: New York, NY, USA, 2014. [[CrossRef](#)]
36. Nelson, D.W.; Sommers, L.E. Total Carbon, Organic Carbon, and Organic Matter. In *Methods of Soil Analysis: Part 3. Chemical Methods*; Sparks, D.L., Page, A.L., Helmke, P.A., Loeppert, R.H., Eds.; Soil Science Society of America and American Society of Agronomy: Madison, WI, USA, 1996; pp. 963–1010. [[CrossRef](#)]
37. Himmelbauer, M.L.; Loiskandl, A.W.; Kastanek, A.F. Estimating length, average diameter and surface area of roots using two different Image analyses systems. *Plant Soil* **2004**, *260*, 111–120. [[CrossRef](#)]
38. Ye, C.; Guo, Z.; Li, Z.; Cai, C. The effect of Bahiagrass roots on soil erosion resistance of Aquults in subtropical China. *Geomorphology* **2017**, *285*, 82–93. [[CrossRef](#)]
39. Wu, X.; Cai, C.; Wang, J.; Wei, Y.; Wang, S. Spatial variations of aggregate stability in relation to sesquioxides for zonal soils, South-central China. *Soil Tillage Res.* **2016**, *157*, 11–22. [[CrossRef](#)]
40. Zhou, M.; Liu, C.; Wang, J.; Meng, Q.; Yuan, Y.; Ma, X.; Liu, X.; Zhu, Y.; Ding, G.; Zhang, J.; et al. Soil aggregates stability and storage of soil organic carbon respond to cropping systems on Black Soils of Northeast China. *Sci. Rep.* **2020**, *10*, 265. [[CrossRef](#)]
41. Dirksen, C. Determination of Soil Water Diffusivity by Sorptivity Measurements. *Soil Sci. Soc. Am. J.* **1975**, *39*, 22–27. [[CrossRef](#)]
42. Dixon, R.M. Design and Use of Closed-top Infiltrometers. *Soil Sci. Soc. Am. J.* **1975**, *39*, 755–763. [[CrossRef](#)]
43. Topp, G.; Zebchuk, W. A closed adjustable head infiltrometer. *Can. Agric. Eng.* **1985**, *27*, 99–104. Available online: <https://eurekamag.com/research/001/283/001283673.php> (accessed on 21 July 2023).
44. Zhu, L.J.; Zhang, G.H.; Ren, Z.P. Comparing four methods for soil infiltration measurement. *Bull. Soil Water Conserv.* **2012**, *32*, 163–167. [[CrossRef](#)]
45. Wooding, R.A. Steady Infiltration from a Shallow Circular Pond. *Water Resour. Res.* **1968**, *4*, 1259–1273. [[CrossRef](#)]
46. Watson, K.W.; Luxmoore, R.J. Estimating Macroporosity in a Forest Watershed by use of a Tension Infiltrometer. *Soil Sci. Soc. Am. J.* **1986**, *50*, 578–582. [[CrossRef](#)]
47. Bodhinayake, W.; Si, B.C.; Xiao, C. New Method for Determining Water-Conducting Macro- and Mesoporosity from Tension Infiltrometer. *Soil Sci. Soc. Am. J.* **2004**, *68*, 760–769. [[CrossRef](#)]
48. Zhu, P.; Zhang, G.; Zhang, B. Soil saturated hydraulic conductivity of typical revegetated plants on steep gully slopes of Chinese Loess Plateau. *Geoderma* **2022**, *412*, 115717. [[CrossRef](#)]
49. Kanwar, R.S.; Rizvi, H.A.; Ahmed, M.; Horton, R.; Marley, S.J. Measurement of Field-Saturated Hydraulic Conductivity by Using Guelph and Velocity Permeameters. *Trans. ASAE* **1990**, *32*, 1885–1890. [[CrossRef](#)]
50. Henseler, J.; Dijkstra, T.K.; Sarstedt, M.; Ringle, C.M.; Diamantopoulos, A.; Straub, D.W.; Ketchen, D.J., Jr.; Hair, J.F.; Hult, G.T.M.; Calantone, R.J. Common Beliefs and Reality About PLS: Comments on Rönkkö and Evermann (2013). *Organ. Res. Methods* **2014**, *17*, 182–209. [[CrossRef](#)]
51. Kostikov, A.N. On the dynamics of the coefficient of water-percolation in soils and on the necessity of studying it from a dynamic point of view for purposes of amelioration, Trans. 6th Cong. International. *Soil Sci. Russ. Part A* **1932**, *14*, 17–21. Available online: <https://cir.nii.ac.jp/crid/1570572699970385664> (accessed on 21 July 2023).
52. Clothier, B.E.; White, I. Measurement of Sorptivity and Soil Water Diffusivity in the Field. *Soil Sci. Soc. Am. J.* **1981**, *45*, 241–245. [[CrossRef](#)]
53. Mao, N.; Huang, L.; Shao, M. Profile distribution of soil saturated hydraulic conductivity and controlling factors under different vegetations on slope in loess region. *Soils* **2019**, *51*, 381–389. [[CrossRef](#)]
54. Franzluebbers, A. Water infiltration and soil structure related to organic matter and its stratification with depth. *Soil Tillage Res.* **2002**, *66*, 197–205. [[CrossRef](#)]
55. Murty, D.; Kirschbaum, M.U.F.; Mcmurtrie, R.E.; Mcgilvray, H. Does conversion of forest to agricultural land change soil carbon and nitrogen? a review of the literature. *Glob. Chang. Biol.* **2002**, *8*, 105–123. [[CrossRef](#)]
56. Neves, C.; Feller, C.; Guimarães, M.; Medina, C.; Filho, J.T.; Fortier, M. Soil bulk density and porosity of homogeneous morphological units identified by the Cropping Profile Method in clayey Oxisols in Brazil. *Soil Tillage Res.* **2003**, *71*, 109–119. [[CrossRef](#)]
57. Basche, A.; DeLonge, M. The Impact of Continuous Living Cover on Soil Hydrologic Properties: A Meta-Analysis. *Soil Sci. Soc. Am. J.* **2017**, *81*, 1179–1190. [[CrossRef](#)]

58. Sun, D.; Yang, H.; Guan, D.; Yang, M.; Wu, J.; Yuan, F.; Jin, C.; Wang, A.; Zhang, Y. The effects of land use change on soil infiltration capacity in China: A meta-analysis. *Sci. Total Environ.* **2018**, *626*, 1394–1401. [\[CrossRef\]](#)
59. Lozano-Baez, S.E.; Cooper, M.; Meli, P.; Ferraz, S.F.; Rodrigues, R.R.; Sauer, T.J. Land restoration by tree planting in the tropics and subtropics improves soil infiltration, but some critical gaps still hinder conclusive results. *For. Ecol. Manag.* **2019**, *444*, 89–95. [\[CrossRef\]](#)
60. Jørgensen, P.R.; Hoffmann, M.; Kistrup, J.P.; Bryde, C.; Bossi, R.; Villholth, K.G. Preferential flow and pesticide transport in a clay-rich till: Field, laboratory, and modeling analysis. *Water Resour. Res.* **2002**, *38*, 28–1-28-15. [\[CrossRef\]](#)
61. Gould, I.J.; Quinton, J.N.; Weigelt, A.; De Deyn, G.B.; Bardgett, R.D. Plant diversity and root traits benefit physical properties key to soil function in grasslands. *Ecol. Lett.* **2016**, *19*, 1140–1149. [\[CrossRef\]](#)
62. Ding, W.-F.; Zhang, X.-C. An evaluation on using soil aggregate stability as the indicator of interrill erodibility. *J. Mt. Sci.* **2016**, *13*, 831–843. [\[CrossRef\]](#)
63. Liu, J.; Zhou, Z.; Su, X. Review of the mechanism of root systems on the formation of soil aggregate. *J. Soil Water Conserv.* **2020**, *34*, 267–273.
64. Su, J.; Zhao, S. Influence of vegetation restoration on distribution of aggregate and organic carbon and nitrogen in Loess Plateau. *Res. Soil Water Conserv.* **2005**, *12*, 44–47. [\[CrossRef\]](#)
65. Cheng, M.; Zhu, Q.; Liu, L.; An, S. Effects of vegetation on soil aggregate stability and organic carbon sequestration in the Ningxia Loess Hilly Region of northwest China. *Acta Ecol. Sin.* **2013**, *33*, 2835–2844. [\[CrossRef\]](#)
66. Li, K.; Palixiati, G.M.; Wang, W.W.; Du, F.; Xu, X.X. Factors influencing water repellency of Heilu soil in Changwu County, Shaanxi Province. *Bull. Soil Water Conserv.* **2021**, *41*, 62–68. [\[CrossRef\]](#)
67. Newton, P.C.D.; Carran, R.A.; Lawrence, E.J. Reduced water repellency of a grassland soil under elevated atmospheric CO₂. *Glob. Chang. Biol.* **2004**, *10*, 1–4. [\[CrossRef\]](#)
68. DeBano, L. The role of fire and soil heating on water repellency in wildland environments: A review. *J. Hydrol.* **2000**, *231–232*, 195–206. [\[CrossRef\]](#)
69. DeBano, L. Water repellency in soils: A historical overview. *J. Hydrol.* **2000**, *231–232*, 4–32. [\[CrossRef\]](#)
70. Yun, H.; Bi, H.; Wang, S.; Zhao, D.; Cui, Y.; Wang, N.; Lan, D. Soil Physical and Chemical Characteristics of Different Forest Types and Their Effects on Soil Infiltration Process, Journal of Soil and Water Conservation. *J. Soil Water Conserv.* **2021**, *35*, 183–189. [\[CrossRef\]](#)
71. Ding, K.; Xu, X.; Chen, W.; Kalhor, S.A. Soil aggregates and infiltration characteristics under different vegetations in Changwu tableland slope of northwestern China. *J. Beijing For. Univ.* **2017**, *39*, 44–51. [\[CrossRef\]](#)
72. Golchin, A.; Oades, J.; Skjemstad, J.; Clarke, P. Soil structure and carbon cycling. *Soil Res.* **1994**, *32*, 1043–1068. [\[CrossRef\]](#)
73. Jastrow, J. Soil aggregate formation and the accrual of particulate and mineral-associated organic matter. *Soil Biol. Biochem.* **1996**, *28*, 665–676. [\[CrossRef\]](#)
74. Six, J.; Elliott, E.; Paustian, K.; Doran, J.W. Aggregation and Soil Organic Matter Accumulation in Cultivated and Native Grassland Soils. *Soil Sci. Soc. Am. J.* **1998**, *62*, 1367–1377. [\[CrossRef\]](#)
75. Six, J.; Bossuyt, H.; Degryze, S.; Deneff, K. A history of research on the link between (micro)aggregates, soil biota, and soil organic matter dynamics. *Soil Tillage Res.* **2004**, *79*, 7–31. [\[CrossRef\]](#)
76. Angers, D.A.; Caron, J. Plant-induced Changes in Soil Structure: Processes and Feedbacks. *Biogeochemistry* **1998**, *42*, 55–72. [\[CrossRef\]](#)
77. Gale, W.; Cambardella, C.; Bailey, T. Root-Derived Carbon and the Formation and Stabilization of Aggregates. *Soil Sci. Soc. Am. J.* **2000**, *64*, 201–207. [\[CrossRef\]](#)
78. Kong, A.Y.Y.; Six, J.; Bryant, D.C.; Denison, R.F.; van Kessel, C. The Relationship between Carbon Input, Aggregation, and Soil Organic Carbon Stabilization in Sustainable Cropping Systems. *Soil Sci. Soc. Am. J.* **2005**, *69*, 1078–1085. [\[CrossRef\]](#)
79. Regelink, I.C.; Stoof, C.R.; Rousseva, S.; Weng, L.; Lair, G.J.; Kram, P.; Nikolaidis, N.P.; Kercheva, M.; Banwart, S.; Comans, R.N. Linkages between aggregate formation, porosity and soil chemical properties. *Geoderma* **2015**, *247–248*, 24–37. [\[CrossRef\]](#)
80. Liu, Y.; Miao, H.; Chang, X.; Wu, G. Higher species diversity improves soil water infiltration capacity by increasing soil organic matter content in semiarid grasslands. *Land Degrad. Dev.* **2019**, *30*, 1599–1606. [\[CrossRef\]](#)
81. Marquart, A.; Eldridge, D.J.; Geissler, K.; Lobas, C.; Blaum, N. Interconnected effects of shrubs, invertebrate-derived macropores and soil texture on water infiltration in a semi-arid savanna rangeland. *Land Degrad. Dev.* **2020**, *31*, 2307–2318. [\[CrossRef\]](#)
82. Guo, L.; Liu, Y.; Wu, G.-L.; Huang, Z.; Cui, Z.; Cheng, Z.; Zhang, R.-Q.; Tian, F.-P.; He, H. Preferential water flow: Influence of alfalfa (*Medicago sativa* L.) decayed root channels on soil water infiltration. *J. Hydrol.* **2019**, *578*, 124019. [\[CrossRef\]](#)
83. Lado, M.; Paz, A.; Ben-Hur, M. Organic Matter and Aggregate-Size Interactions in Saturated Hydraulic Conductivity. *Soil Sci. Soc. Am. J.* **2004**, *68*, 234–242. [\[CrossRef\]](#)
84. Fu, T.; Chen, H.; Zhang, W.; Nie, Y.; Wang, K. Vertical distribution of soil saturated hydraulic conductivity and its influencing factors in a small karst catchment in Southwest China. *Environ. Monit. Assess.* **2015**, *187*, 92. [\[CrossRef\]](#) [\[PubMed\]](#)
85. Yang, F.-S.; Cao, M.-M.; Li, H.-E.; Wang, X.-H.; Bi, C.-F. Simulation of sediment retention effects of the single seabuckthorn flexible dam in the Pisha Sandstone area. *Ecol. Eng.* **2013**, *52*, 228–237. [\[CrossRef\]](#)
86. Shi, Y.; Ye, H.; Hou, H.; Bi, Z. The Internal Cause of the Erosion in “Pisha” Sandstone Area, Southern Inner Mongolia. *Acta Geosci. Sin.* **2004**, *25*, 659–664. [\[CrossRef\]](#)

87. Logsdon, S.D.; Allmaras, R.R. Maize and soybean root clustering as indicated by root mapping. *Plant Soil* **1991**, *131*, 169–176. [[CrossRef](#)]
88. Wu, T.-N.; Wu, G.-L.; Wang, D.; Shi, Z.-H. Soil-hydrological properties response to grazing exclusion in a steppe grassland of the Loess Plateau. *Environ. Earth Sci.* **2013**, *71*, 745–752. [[CrossRef](#)]
89. Liu, Y.; Cui, Z.; Huang, Z.; López-Vicente, M.; Wu, G.-L. Influence of soil moisture and plant roots on the soil infiltration capacity at different stages in arid grasslands of China. *Catena* **2019**, *182*, 104147. [[CrossRef](#)]
90. Gamie, R.; De Smedt, F. Experimental and statistical study of saturated hydraulic conductivity and relations with other soil properties of a desert soil. *Eur. J. Soil Sci.* **2017**, *69*, 256–264. [[CrossRef](#)]
91. Liu, S.; Wang, Y.; An, Z.; Sun, H.; Zhang, P.; Zhao, Y.; Zhou, Z.; Xu, L.; Zhou, J.; Qi, L. Watershed spatial heterogeneity of soil saturated hydraulic conductivity as affected by landscape unit in the critical zone. *Catena* **2021**, *203*, 105322. [[CrossRef](#)]

Disclaimer/Publisher’s Note: The statements, opinions and data contained in all publications are solely those of the individual author(s) and contributor(s) and not of MDPI and/or the editor(s). MDPI and/or the editor(s) disclaim responsibility for any injury to people or property resulting from any ideas, methods, instructions or products referred to in the content.